TSC and Broadband Dielectric Spectroscopy Studies of the α Relaxation in Phosphorus-Containing Dendrimers

E. Dantras,* J. Dandurand, and C. Lacabanne

Laboratoire de Physique des Polymères, CIRIMAT, Université Paul Sabatier, 31062 Toulouse Cedex 04, France

A. M. Caminade and J. P. Majoral

Laboratoire de Chimie de Coordination, 31077 Toulouse Cedex 04, France

Received January 6, 2004; Revised Manuscript Received February 20, 2004

ABSTRACT: The aim of this work is to analyze the dielectric manifestation of the glass transition (α mode) of amorphous dendritic macromolecules as a function of architectural complexity. A set of phosphorus-containing dendrimers involving six generations ($g = 0-5$) has been investigated by thermostimulated currents and broadband dielectric spectroscopy. The dielectric complex permittivity has been obtained as a function of temperature, in a broad frequency range ($10^{-4}-10^{6}$ Hz). For frequencies higher than 1 Hz, the dendrimers show a high temperature α mode with a Vogel−Tamman−Fulcher type temperature dependence. For frequencies lower than 1 Hz, the α mode takes place in the vitreous state; it has been associated with a series of thermally activated cooperative movements free from generation influence. Dielectric and thermal properties are discussed as regards of fractal architecture and chemical modification of end groups.

Introduction

Glass transition,[1] physical aging,[2] mechanical studies,[3,4] and low-temperature dynamics[5] have been already described in dendrimers literature. However, up to now, the molecular mobility near the glass transition, with a large dendrimer series, remains unexplored due to conductivity phenomenom. In this work, we focus on generation from $g = 0$ to $g = 5$, of amorphous phosphorus-containing dendrimers, with chemical modifications of end groups. The phosphorus-containing dendrimers series has been chosen as a complex polymeric model to investigate the relationship between complex α relaxation modes with a specific architecture. The aim of this work is to analyze the influence of architecture on α molecular mobility upon increasing generation. Thanks to complementary dielectric techniques as thermostimulated currents (TSC) and broadband dielectric spectroscopy (BDS), the mechanism of dipolar polarization and its evolution as a function of the generation of dendrimers may be studied. As previously shown for the β mode,[6] we follow the shift of α relaxation modes on a wide frequency and temperature range.

Experimental Section

Materials: Phosphorus-Containing Dendrimers. The synthesis of phosphorus-containing dendrimers consists of the repetition of two steps, starting from a core having phosphorus−chlorine bonds, such as $P(S)Cl_3$. The first step is the nucleophilic substitution of chlorine by hydroxy-benzaldehyde leading to a trialdehyde. The second step is the condensation of the aldehydes with $H_2NMeP(S)Cl_2$. This reaction induces the multiplication of the number of end groups, with phosphorus acting as the divergent point. The repetition of these two steps allows us to build the dendrimer. Details of this synthesis and various characterizations of these amorphous polymers were described elsewhere.[7−9] Numbering of these compounds hereafter will be done as follows: $[G'_g]$, where g is the number of generation−here $g = 0$, ..., 5−and G' corresponds to dendrimers with terminal aldehyde end groups (G corresponds to dendrimers without terminal aldehyde end groups). The 3d molecular structures of phosphorus-containing dendrimers with a cauliflower architecture are illustrated in Figure 1. For sake of simplicity, we limit the figure to $g = 0$ and $g = 3$. All the studied samples are available as powder. To eliminate the remaining traces of free solvent molecules (THF), the samples have been heated at $T_g + 30$ °C under a pressure of 10^{-5} hPa for 30 min. The micro-Brownian movements liberated at such temperatures might allow the diffusion of such molecules.

Methods: Isothermal Broadband Dielectric Spectroscopy and Thermostimulated Currents. In the case of BDS, the sample is constituted by a thin layer of powder (100 ± 10 μm). For TSC experiments, slightly compressed pellets of 800 ± 10 μm thick were directly inserted between electrodes. Broadband dielectric measurements were performed using a NOVOCONTROL BDS400 covering a frequency range of 10^{-2} Hz/3 × 10^{6} Hz with 10 points per decade. Experiments were carried out within a temperature range 70 °C/175 °C. Dielectric isotherm spectra were measured every 5 °C. Before each frequency scan, temperature was kept constant to within ±0.2 °C. The real ϵ'_T and imaginary ϵ''_T parts of the relative complex permittivity ϵ^*_T, were measured as a function of frequency F at a given temperature T. Experimental data are fitted by the Havriliak−Negami (HN) function with an additional conductivity term:[10,11]

$$\epsilon^*_{\mathbf{T}}(\omega) = \epsilon_\infty + \frac{\epsilon_{st} - \epsilon_\infty}{[\mathbf{1} + (\mathbf{i}\omega\tau_{\mathbf{HN}})^{\alpha_{HN}}]^{\beta_{HN}}} - \mathbf{i}\left(\frac{\sigma_0}{\epsilon_0\omega}\right)^{\mathbf{n}} \qquad (1)$$

where ϵ_∞ is the relative real permittivity at infinite frequency, ϵ_{st} is the relative real permittivity at null frequency, ϵ_0 is the permittivity of vacuum, τ_{HN} is the relaxation time, ω is the angular frequency, and α_{HN} and β_{HN} are the Havriliak−Negami parameters. To obtain dielectric loss free from ohmic conduction, we calculate from the real part $\epsilon'_T(\omega)$, ϵ''_{KK} with Kramers−Kronig relationships (KK):

$$\epsilon''_{KK}(\omega_0) = \left(\frac{\sigma_0}{\epsilon_0\omega_0}\right) + \frac{2}{\pi}\int_0^\infty \epsilon'(\omega)\frac{\omega_0}{\omega^2 - {\omega_0}^2}\mathrm{d}\omega \qquad (2)$$

We have used numerical techniques described in ref 12.

* Corresponding author. E-mail: dantras@cict.fr.

10.1021/ma049955i CCC: $27.50
Published on Web 03/24/2004

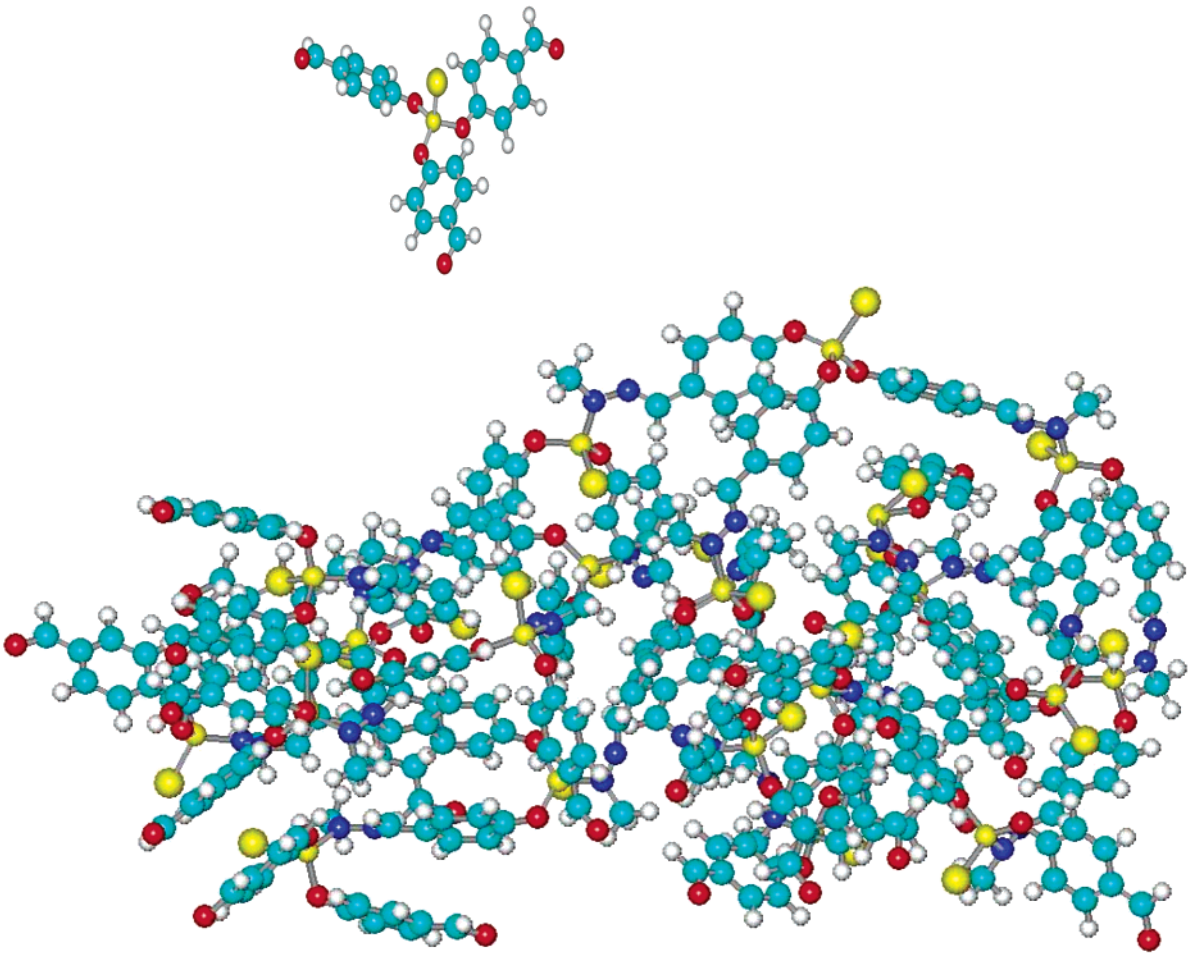

Figure 1. Molecular architecture of $[G'_0]$ and $[G'_3]$ (yellow sphere, sulfur atom; small yellow sphere, phosphorus atom; dark blue sphere, nitrogen atom; blue sphere, carbon atom; white sphere, hydrogen atom).

Complex TSC spectra and fractional polarization analysis were carried out on a TSC/RMA analyzer. For global experiments, the sample was polarized by an electrostatic field $E_p = 400$ kV·m^{-1} during $t_p = 2$ min over a temperature range from the polarization temperature, T_p, down to the freezing temperature, $T_0 = 0$ °C. Then, the field was turned off and the depolarization current was recorded with a constant heating rate ($q_h = +7$ °C·min^{-1}), so that the equivalent frequency of the TSC spectrum was $f_{eq} \sim 10^{-3}$–10^{-4} Hz. TSC experiments are complementary from BDS spectroscopy on the low-frequency side. For windowing experiments (*i*th elementary peak), the polarizing field was applied for $t_p = 2$min at T_p^i. Then, the sample was short-circuited at $T_d^i = T_p^i - \Delta T_p$ and the temperature maintained constant for $t_d = t_p$. Finally, the sample was cooled at $T_0^i = T_p^i - 50$ °C, and the depolarization current was recorded in the same way as for the complex mode. Windowing experiments were carried out:[13,14] narrow poling windows ($\Delta T_p \leq 5$ °C) are used for isolating elementary processes that can be analyzed with the hypothesis of a single relaxation time. Details of BDS and TSC techniques have been published in ref 15.

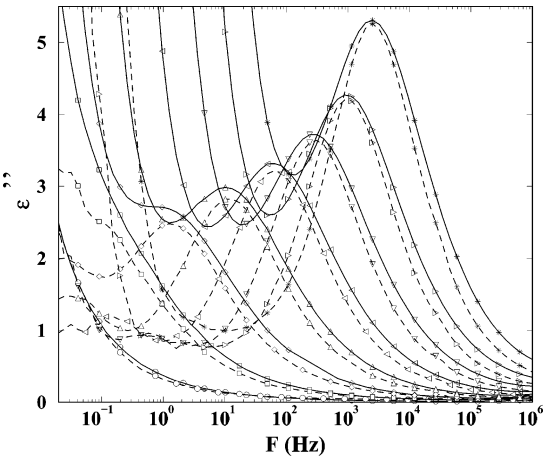

Figure 2. Frequency dependence of the dielectric energy loss $\epsilon''_T(\omega)$ (solid lines) for the α-mode of $[G'_1]$ and $\epsilon''_{KK}(\omega)$ (dashed line) calculated from $\epsilon'_T(\omega)$.

Results and Discussion

Isothermal Response. Broadband Dielectric Spectroscopy of α Relaxation Mode. Phosphorus-containing dendrimers exhibit one primary relaxation region labeled α. Figure 2 (solid lines) shows the α mode for $[G'_1]$ as example. The strength of this α mode increases vs temperature. This dipolar relaxation is associated with the dielectric manifestation of the glass transition observed near $T_g([G'_1]) = 69.3$ °C by DSC (obtained during cooling with $q_c = -5$ °C·min^{-1}). For the isotherm $T = 70$ °C, the conductivity contribution appears on the low frequency tail of $\epsilon''_T(\omega)$. Note that dielectric manifestation of glass transition cannot be easily observed for middle and high generation, due to superimposed conductivity phenomenom. We also report in Figure 2 (dashed lines), $\epsilon''_{KK}(\omega)$ where the ohmic conduction has been eliminated. We observe a good agreement between $\epsilon''_{KK}(\omega)$ and measured $\epsilon''_T(\omega)$ for the α relaxation mode of $[G'_1]$ except at low frequencies when the two curves deviate due to conduction losses

Table 1. Havriliak−Negami Parameters Deduced from the Fit for [G_1']

	T (°C)	σ_0 (S·cm^{-1})	n	τ (s)	$\Delta\epsilon = \epsilon_{st} - \epsilon_\infty$	α_{HN}	β_{HN}
$\epsilon_T''(\omega)$	80	1.5×10^{-13}	0.89	1.1×10^{-1}	10.5	0.6	0.8
$\epsilon_{KK}''(\omega)$				1.5×10^{-1}	10.7	0.5	1
$\epsilon_T''(\omega)$	85	5×10^{-13}	0.99	1.4×10^{-2}	12.4	0.6	1
$\epsilon_{KK}''(\omega)$				1.7×10^{-2}	10.6	0.6	0.9
$\epsilon_T''(\omega)$	90	2.5×10^{-12}	0.94	2.5×10^{-3}	12.6	0.7	0.7
$\epsilon_{KK}''(\omega)$				2.8×10^{-3}	11.5	0.7	0.9
$\epsilon_T''(\omega)$	95	9×10^{-12}	0.95	5.6×10^{-4}	14	0.7	0.8
$\epsilon_{KK}''(\omega)$				6.2×10^{-4}	12.6	0.7	0.9
$\epsilon_T''(\omega)$	100	3.1×10^{-11}	0.91	1.7×10^{-4}	15.6	0.7	0.7
$\epsilon_{KK}''(\omega)$				1.7×10^{-4}	15	0.6	1
$\epsilon_T''(\omega)$	105	8.5×10^{-11}	0.91	6.6×10^{-5}	19.6	0.7	0.75
$\epsilon_{KK}''(\omega)$				6.4×10^{-5}	18	0.7	1

in $\epsilon_T''(\omega)$. Experimental and calculated dielectric data are fitted with HN equation (see eq 1 for experimental data with a conductivity term) and the n, α_{HN}, and β_{HN} values are reported in Table 1. In the case of experimental data, parameter n is quasi-equal to 1, which is characteristic of an ohmic conductivity. The global shape of the α mode is practically independent of temperature. For calculated data deduced from the Kramers−Kronig equation, we note the close values for τ, $\Delta\epsilon$, and α_{HN} compared with Havriliak−Negami data extracted from experimental data. In contrast, a nearly constant $\beta_{HN} \sim 1$ for $\epsilon_{KK}''(\omega)$ is obtained over the temperature range. α modes of phosphorus-containing dendrimers are well described by a Cole−Cole phenomenological model. We note that the relaxation strength of the α process at various temperatures is higher than typically observed in amorphous polymers. The major architectural difference that might explain this result is the small length of the dendrons (<16 Å for $g = 1$) with polar ends. Consequently the polar species have a much higher molecular mobility, increasing signicantly their contribution to the dielectric permittivity.

Temperature Dependence of Dielectric Relaxation Times. Figure 3 compares the relaxation times for $\epsilon_T''(\omega)$ and $\epsilon_{KK}''(\omega)$ of the α mode of [G_1'] at different temperatures. Both show the same temperature dependence. As for most polymers,[16] the primary mode of phosphorus-containing dendrimers is well described by a Vogel−Tamman−Fulcher (VTF) equation.

$$\tau_{HN}(T) = \tau_0 \exp\left(\frac{1}{\alpha_f(T - T_\infty)}\right) \quad (3)$$

The adjustable parameters τ_0, α_f, and T_∞ depend on polymer. This equation (or the empirical WLF equation) offers a semiempirical mean of accommodating the nonarrhenian temperature dependence of relaxation times. The parameter τ_0 is the value of $\tau_{HN}(T)$ at infinite temperature, and T_∞ is the temperature corresponding to an infinite relaxation time. The parameter α_f designates the free volume expansion coefficient. VTF parameters are reported in Table 2. We note that α_f parameter is more important (×10) than commonly reported values for a wide variety of polymers, which is probably due to the specific architecture of dendrimers.

Thermostimulated Response. TSC Thermogram of the α Relaxation Mode. The TSC global spectrum of dendrimers is shown in Figure 4. The polarizing field of 4×10^5 V·m^{-1} was applied at poling temperatures indicated by small arrows. Then the sample was quenched to 0 °C and heated again at 7 °C·min^{-1}.

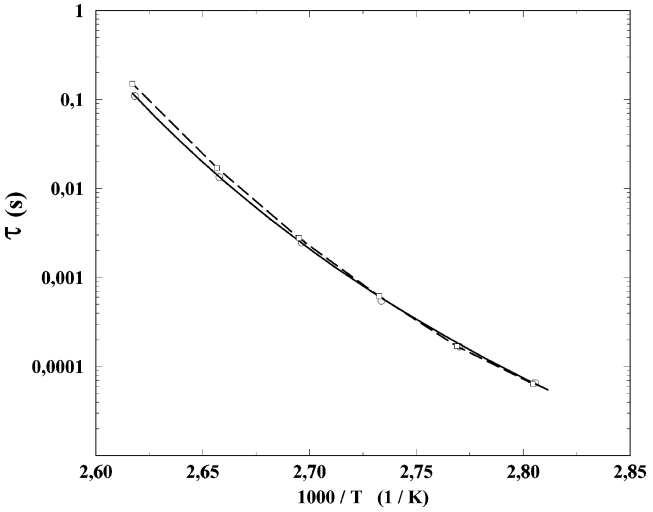

Figure 3. Vogel dependence of τ_{HN} for the α-mode of [G_1']: experimental points (○) with fit shown by the solid line and calculated points from KK (□) with fit shown by the dashed line.

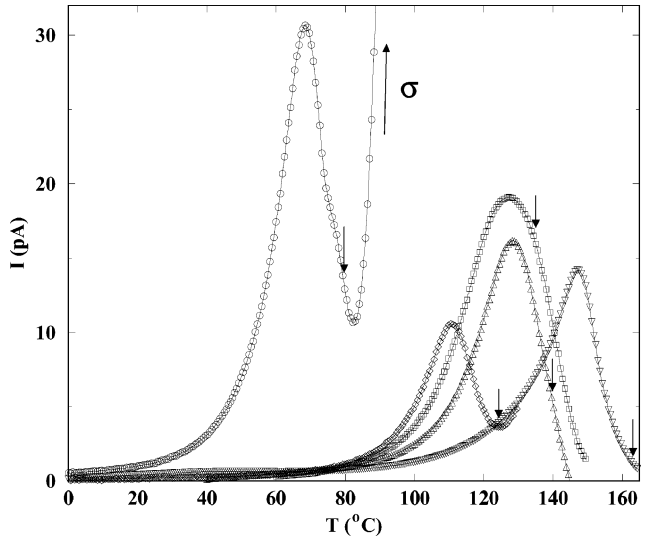

Figure 4. Depolarization currents vs temperature for [G_1'] to [G_5']: [G_1'] indicated by ○, [G_{23}'] by □, [G_3'] by ◇, [G_4'] by △, and [G_5'] by ▽.

Table 2. Vogel−Tammann−Fulcher Parameters for the Generation [G_1'] Deduced from the Fit

τ_0 (s)	α_f (K^{-1})	T_∞ (K)
1.25×10^{-10}	1.1×10^{-3}	309

Dielectric manifestation of the glass transition are recorded between 60 °C/150 °C with 10 pA ≤ I_{max} ≤ 30 pA. I_{max} is quasi-independent from generation since the dipole's number/volume ratio is constant due to self-similarity. Contrarily, $T_\alpha([G_g'])$ is dependent from generation. One hypothesis that might explain this evolution is the presence of solvent molecules trapped during synthesis. Indeed such trapping has been recently shown by Majoral et al.[17] To permit the elimination of such a molecule, we need to heat the sample at a temperature where the global molecule is mobile: by analogy with polymers we might think that at some T_g + 50 °C, we reach such mobility. So the sample has been heated at such temperature under vacuum as shown in Figure 5. A shift of TSC peaks toward higher temperatures indicate the departure of trapped mol-

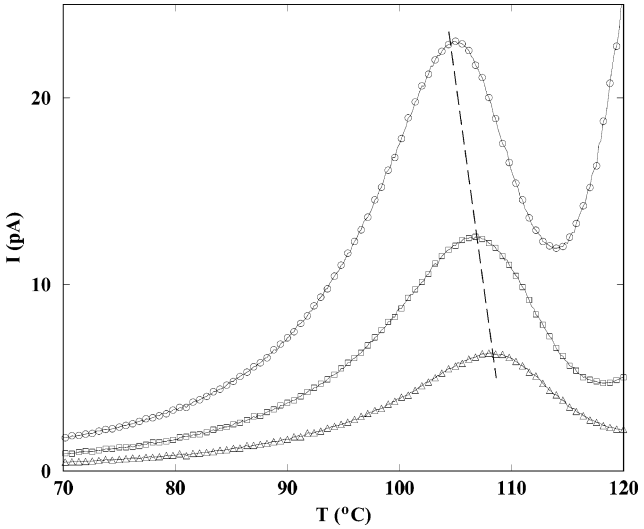

Figure 5. Antiplasticization phenomenon for $[G'_3]$: the first annealing ($T_g + 50$ °C) and pumping indicated by ○, the second one indicated by □, and the third one indicated by △.

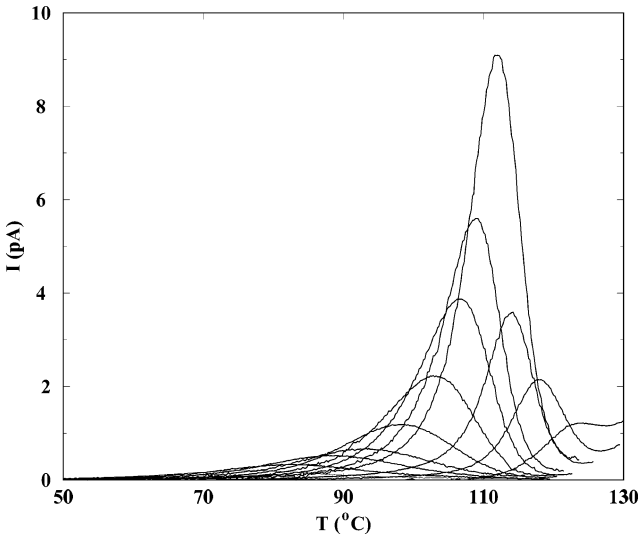

Figure 6. Elementary spectra obtained for $[G'_3]$.

ecules. Such an antiplasticization effect under extraction of the solvent molecule validates the contribution of the cage molecule in the evolution of TSC peaks upon generation. This experimental behavior illustrates cage molecule properties (facilities for trapping) of dendrimers architecture. In the case of $[G'_1]$, a second contribution is pointed out: a conductivity phenomena called σ. This electronic disturbance is probably responsible for I_{max} increases (until 30 pA).

Discrete Distribution of Relaxation Times for α Relaxation Mode The resolution of the fine structure of complex spectra has been performed by using fractional polarizations. Elementary spectra are reported in Figure 6 for $[G'_3]$ as example. The polarization window of 5 °C was shifted along the temperature axis by 5 °C for the α mode. These elementary spectra can be analyzed by assuming the existence of a single relaxation time. This allows us to define the activation enthalpy variation as a function of the activation entropy for each isolated process. Activation parameters deduced from each elementary spectrum analysis are reported in Table 3 for the series from $[G'_1]$ to $[G'_5]$. According to the usual behavior of activation parameters isolated in the α mode of polymeric materials, we have

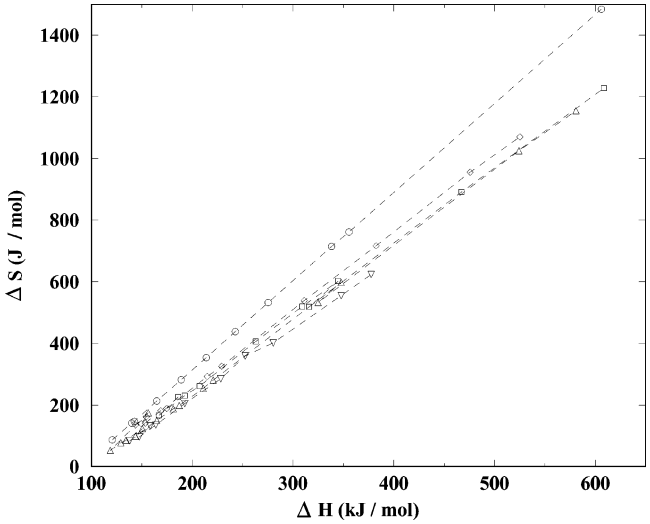

Figure 7. Meyer−Neldel law for $[G'_1]$ to $[G'_5]$: $[G'_1]$ indicated by ○, $[G'_2]$ by □, $[G'_3]$ by ◇, $[G'_4]$ by △, and $[G'_5]$ by ▽.

Table 3. Activation Parameters Deduced from Elementary Spectra Analysis

generation	$g = 1$	$g = 2$	$g = 3$	$g = 4$	$g = 5$
T_g (°C)	69	124	125	149	159
T_c (°C)	74	138	125	140	163
$\lvert\Delta(T_c - T_g)\rvert$ (°C)	5	14	0	9	4
ΔH_{max} (kJ·mol^{-1})	606	609	534	581	378
ΔH_{min} (kJ·mol^{-1})	121	186	146	119	138
$r = (\Delta H_{max}/\Delta H_{min})$	5	3.3	3.7	5	2.7

plotted ΔS and ΔH on a compensation diagram as shown in Figure 7. We note that the compensation temperature T_c is slightly above the glass transition temperature T_g for the series of dendrimers. This point is consistent with previous works[18] on a poly(methyl methacrylate) series with increasing M_w. A compensation law, also called the Meyer−Neldel law, is observed. It is characteristic of the cooperativity of the α mode in phosphorus-containing dendrimers. We note also that enthalpy range is independent from generation (Figure 7 and Table 3): ΔH always increases, and it is multiplied by a factor ranging from 5 to 2.7. It was already shown[19] that the enthalpy range (ΔH_{max}, ΔH_{min}) is characteristic of the dispersion of the relaxing units length. This enthalpy range $\Delta H_{max} - \Delta H_{min}$ remains of the same order of magnitude independently from generation: it means that cooperatively rearranging regions having the same size distribution are explored. As phosphorus-containing dendrimers are characterized by a fractal architecture (Cayley tree): it means that the α relaxation mode takes place in self-similar neighboring domains (Figure 8). Experiments carried out on $[G'_1]$ (dendrimers with aldehyde end groups) and $[G_1]$ (dendrimers without aldehyde end groups) show that α mode is quasi-independent from the aldehyde groups. This comparative study shows that end groups are not implied in α relaxation mode. In a previous work,[6] we have shown that the aldehyde end groups are responsible for the low-temperature β relaxation mode. When the number of generations increases, glass transition temperatures increase with topological interactions. The same shift is observed for the α relaxation mode associated with the dielectric manifestation of the glass transition. Broad compensation phenomena analogous with those observed in polymers indicated the existence of a wide distribution of cooperatively rearranging regions (CRR), where molecular mobility takes place.

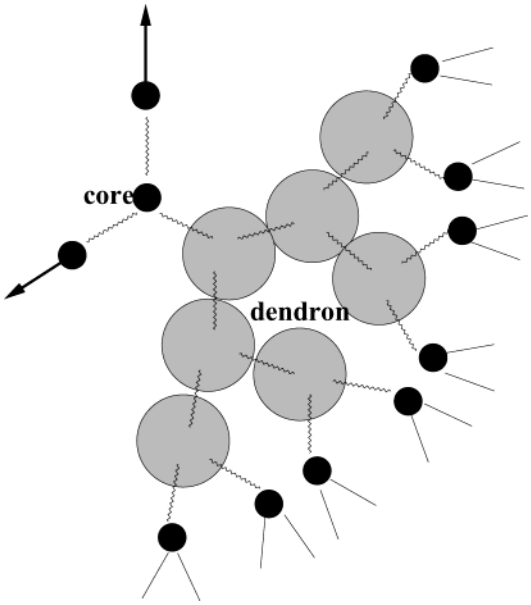

Figure 8. Schematic representation of a dendron with relaxation domains (shaded areas).

It is important to note that neither the mobility of end groups nor the generation of dendrimers is implied.

Conclusion

The synergy of isothermal dielectric spectroscopy with thermostimulated currents analysis, underlined in a previous work,[20] has allowed us to explore the cooperative molecular mobility liberated around the glass transition in dendrimers. To achieve a more complete analysis of the dynamics of the α relaxation mode, the Kramers−Kronig transform has been used. The molecular mobility observed for frequencies higher than 1 Hz, exhibits a VTF behavior indicating an increase of the "apparent activation enthalpy" as the temperatures approach T_g. Then, following Donth's model,[21,22] this behavior can be assigned to an increase of the size of domains where molecular mobility takes place. For frequency of some 10^{-2} Hz, the α relaxation mode is observed below T_g i.e., in the vitreous state. Then, the α relaxation mode is due to a series of thermally activated processes involving various dendrons sequences: the domains where the molecular mobility takes place are frozen, and their size distribution is reflected by the width of the distribution of activation enthalpy. The metastability of the vitreous state is responsible for structural relaxation. Some 100 °C below T_g, those domains behave as rigid hard spheres. A localized molecular mobility is responsible for a β relaxation mode described elsewhere.[6] It has been assigned to the local mobility of aldehydes situated at dendron ends. Such mobility of dendron ends has been related to a peculiar surface reactivity of dendrimers.

References and Notes

(1) Wooley, K. L.; Hawker, C. J.; Pochan, J. M.; Fréchet, J. M. J. *Macromolecules* **1993**, *26*, 1514−1519.
(2) Dantras, E.; Dandurand, J.; Caminade, A. M.; Majoral, J. P.; Lacabanne, C. *Macromolecules* **2002**, *35*, 2090−2094.
(3) Sendijarevic, I.; McHugh, A. J. *Macromolecules* **2000**, *33*, 590−596.
(4) Uppulari, S.; Morrison, F. A.; Dvornic, P. R. *Macromolecules* **2000**, *33*, 2551−2560.
(5) Huwe, A.; Appelhans, D.; Prigann, J.; Voit, B. I.; Kremer, F. *Macromolecules* **2000**, *33*, 3762−3766.
(6) Dantras, E.; Caminade, A. M.; Majoral, J. P.; Lacabanne, C. *Macromolecules* **2001**, *34*, 3808−3811.
(7) Lartigue, M. L.; Donnadieu, B.; Galliot, G.; Caminade, A.-M.; Majoral, J.-P.; Fayet, J.-P. *Macromolecules* **1997**, *30*, 7335−7337.
(8) Majoral, J.-P.; Caminade, A.-M. *Top. Curr. Chem.* **1998**, *197*, 79−124.
(9) Turrin, C.-O.; Maraval, V.; Leclaire, J.; Dantras, E.; Lacabanne, C.; Caminade, A.-M; Majoral, J.-P. *Tetrahedron* **2003**, *59*, 3965−3973.
(10) Havriliak, S.; Negami, S. *J. Polym. Sci., Part C* **1966**, *14*, 99−117.
(11) Havriliak, S.; Negami, S. J. *Polymer* **1967**, *8*, 161−210.
(12) Steeman, P. A. M.; van Turnhout, J. *Colloid Polym. Sci.* **1997**, *275*, 106−115.
(13) Chatain, D.; Gautier, P.; Lacabanne, C. *J. Polym. Sci., Phys. Ed.* **1973**, *11*, 1631−1640.
(14) Teyssèdre, G.; Lacabanne, C. *J. Phys. D, Appl. Phys.* **1995**, *28*, 1478−1487.
(15) Runt, J. P.; Fitzgerald, J. J. *Dielectric spectroscopy of polymeric materials: Fundamentals and Applications*; American Chemical Society: Washington, DC, 1997; p 8.
(16) McCrum, N.; G.; Read, B.; E.; Williams, G. *Anelastic and dielectric effects in polymeric solids*; J. Wiley: New York, 1991.
(17) Leclaire, J.; Coppel, Y.; Caminade, A.-M.; Majoral, J.-P., submitted for publication in *J. Am. Chem. Soc.* **2004**.
(18) Doulut, S.; Bacharan, C.; Demont, P.; Bernès, A.; Lacabanne, C. *J. Non-Cryst. Solids* **1998**, *235−237*, 645−651.
(19) Samouillan, V.; Lamure, A.; Maurel, E.; Lacabanne, L.; Hornebeck, W. *Biopolymers* **2001**, *58*, 175−185.
(20) Dantras, E.; Dudognon, E.; Samouillan, V.; Menegotto, J.; Bernès, A.; Demont, P.; Lacabanne, C. *J. Non-Cryst. Solids* **2002**, *307−310*, 671−678.
(21) Donth, E. *J. Non-Cryst. Solids* **1982**, *53*, 325−330.
(22) Fischer, E. W.; Donth, E.; Steffen, W. *Phys. Rev. Lett.* **1992**, *68*, 2344−2346.

MA049955I